ELSEVIER

Signal Processing 80 (2000) 1833–1847

SIGNAL PROCESSING

www.elsevier.nl/locate/sigpro

Radar fusion to detect dim targets

A. Farina[a,*], M. Grazzini[b]

[a] *Alenia Marconi Systems, Systems Analysis Group, Via Tiburtina Km. 12.400, 00131 Rome, Italy*
[b] *Elettronica SpA, Via Tiburtina Km. 13.700, 00131 Rome, Italy*

Received 4 January 2000; received in revised form 7 March 2000

Abstract

This paper explores the benefit of combining the data of a microwave phased-array radar with those of a low-frequency radar to detect and track a target with a low radar cross-section. The microwave phased-array radar has a fairly good target location accuracy that can be fruitfully combined with the good detection capabilities of the low-frequency radar. One technical problem to solve is the determination of the carrier of the low-frequency radar; this paper highlights a technical procedure to solve the problem. Another technical problem of interest is the evaluation of the benefit gained in fusing the data from two radar having such different carrier frequencies. A detailed numerical example shows the benefit in terms of detection and track range values with respect to the cases of using either the microwave radar (X-band in the numerical exercise) alone or the low-frequency radar (UHF-band in the numerical exercise) alone.

Zusammenfassung

Dieser Artikel untersucht den Nutzen, der sich aus der Kombination von Daten eines Mikrowellenradars mit phasengesteuerter Sensorgruppe mit den Daten eines Niederfrequenzradars im Hinblick auf die Detektion und Verfolgung eines Zieles mit geringem Radarquerschnitt ergibt. Das phasengesteuerte Mikrowellenradar besitzt eine akzeptable Zielortungsgenauigkeit, die vorteilhaft mit der guten Deterktionsfähigkeit des Niederfrequenzradars kombiniert werden kann. Ein zu lösendes technisches Problem besteht allerdings in der Bestimmung des Trägers des Niederfrequenzradars. Dieser Artikel stellt ein Verfahren vor, um dieses Problem zu lösen. Eine weitere Schwierigkeit liegt in der Bewertung des Nutzens, der sich aus der Verbindung der Daten zweier Radarsysteme mit so unterschiedlichen Trägerfrequenzen ergibt. Ein detailliertes numerisches Beispiel zeigt den Gewinn im Hinblick auf Detektion und Entfernungsbestimmung im Vergleich zu Fällen, in denen jeweils ausschließlich das Mikrowellenradar (X-Band im numerischen Beispiel) oder das Niederfrequenzradar (UHF-Band im numerischen Beispiel) verwendet wird.

Résumé

Nous explorons dans cet article le bénéfice à combiner les données d'un radar de type réseau phasé micro-ondes avec celles d'un radar basse-fréquence pour la détection et la poursuite de cible avec une section radar faible. Le radar de type réseau phasé micro-ondes offre une précison de localisation de cible passablement bonne, pouvant être combinée fructueusement avec les bonnes capacités de détection du radar basse-fréquence. Un problème technique à régler est celui de la détermination de la porteuse du radar basse-fréquence; Cet article met en Jumière une procédure technique pour

* Corresponding author. Tel.: + 39-06-4150-2279; fax: + 39-06-4150-2665.
E-mail addresses: farina@alenia.finmeccanica.it, afarina@aleniasystems.finmeccanica.it (A. Farina), eltya@tin.it (M. Grazzini).

0165-1684/00/$ - see front matter
PII: S0165-1684(00)00092-X

résoudre ce problème. Une autre problème technique intéressant est celui de l'évaluation du bénéfice acquis en fusionnant les données de duex radars ayant des fréquences porteuses différentes. Un exemple numérique détaillé montre le bénéfice en termes de détection et de poursuite vis-à-vis des cas où le radar micro-ondes (bande X en l'occurrence) seul ou le radar basse-fréquence (bande UHF en l'occurrence) seul est utilisé.

Keywords: Radar; Fusion; Cueing; Low-frequency radar

Nomenclature

A_e	effective antenna aperture area
d	effective antenna aperture length
h_{tgt}	target height above the earth surface
h_R	height of the radar antenna phase centre above the earth surface
L	global losses of radar
P_D	target detection probability
P_{FA}	probability of false alarm
P_t	average transmitted power of radar
R_h	maximum radar range in the presence of a spherical earth
R_m	maximum radar range in the presence of multipath
R_{max}	maximum radar range
t_f	refresh time period for a given angular sector Ω_o
S_{min}	minimum signal-to-noise power ratio to obtain a specified value of P_D for a certain value of P_{FA}
T	noise temperature (K) of the radar receiver
U_s	time fraction of MR dedicated to search
Ω	search volume in which LFR has detected the target
Ω_o	overall radar search volume
θ_B	half-power beam width
λ	wavelength of radar electromagnetic wave
σ	target radar cross-section
σ_θ	standard deviation of angle measurement

Acronyms

LFR	low-frequency radar
MR	microwave phased-array radar
RCS	radar cross section of target
SNR	signal-to-noise power ratio

1. Problem statement and description of system fusion

Modern radar systems are tasked of detecting and tracking dim targets, i.e., targets with low radar cross section (RCS, also indicated with σ in the following). The reduction of RCS is possible by resorting to proper technologies (see [1, pp. 413–485] for a survey description of these). Target with low RCS are difficult to detect and track because of the corresponding low value of the signal-to-noise power ratio (SNR) in the radar receiver. This paper presents a design concept to detect and track dim target. The rationale of the system is to use a microwave phased-array radar (MR) in conjunction with a low-frequency radar (LFR). It is known that at low frequency the target RCS is greater than at microwaves; in fact, the technologies to reduce the target RCS are less effective at low frequency. Consequently, the LFR has improved target detection capability. The drawback is that the location accuracy of the target is poor because the beam width of a low-frequency radar is wide. Conversely, a microwave radar has difficulties in detecting a target because the techniques to reduce the target RCS are, in principle, quite effective in the microwave region of the electromagnetic spectrum. Nevertheless, if the target is

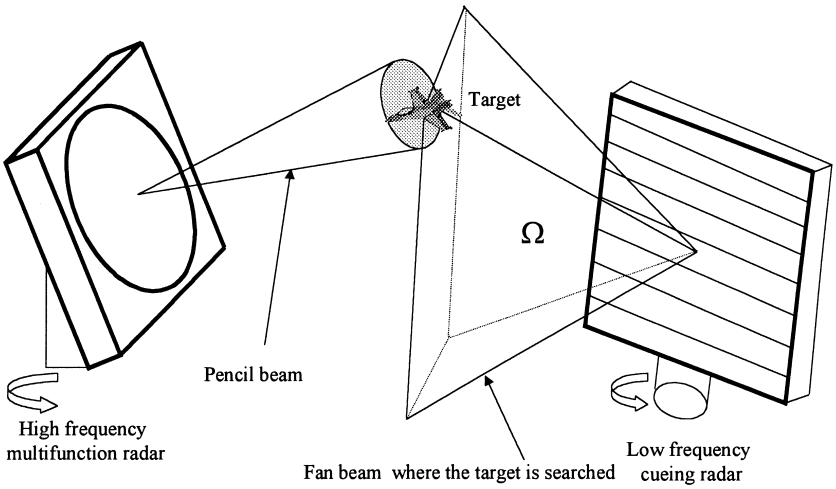

Fig. 1. The joint operation of a phased-array microwave radar and a low-frequency radar.

detected in some way (for instance, by using the low-frequency radar), the target can be accurately tracked by exploiting the good location capabilities of the microwave radar.

The system to study in this paper is displayed in Fig. 1. It is composed of an MR (it is a rotating phased-array radar with narrow beam) and a rotating LFR (the carrier frequency is a parameter to determine during the study). The LFR detects the target at a distance greater than the distance at which the target could be detected by the MR; however, the LFR has a wide beam thus the location accuracy of the target is poor. The MR is cued onto the sector Ω where the LFR has detected the target. The MR concentrates the search in that sector by sweeping the narrow beam across it; when the target is detected the corresponding location accuracy is the one related to the beam width of the MR.

The working procedure of the integrated system, the selection of the LFR carrier frequency and the evaluation of the advantage of the sensor fusion, are presented in the technical material that follows. In the next section, we describe the behaviour of the target RCS as a function of the frequency; the purpose is to show the considerable difference in numerical value of the RCS in the microwave and low frequency regions. Subsequently, the sensor fusion problem is illustrated in Section 3. The detection capability of each sensor operating in stand alone mode and of the combined system is the subject of Section 4. Section 5 presents the range for track initiation, while Section 6 determines the range at which the track has reached a prescribed cross-range accuracy. An analysis of the multipath phenomenon that limits the LFR performance is the subject of Section 7. Concluding remarks (Section 8) close the paper.

2. Target RCS versus frequency

We describe the case of conventional target and briefly consider the case of a target that exploits the techniques to reduce its RCS.

When an object is illuminated by an electromagnetic wave, electric currents and magnetic fields are induced on and within it according to Maxwell's equations and the appropriate boundary conditions. These induced currents and fields, in turn, act as sources on an antenna and generate an electromagnetic field of their own. This is the field scattered by the object, and is generally radiated in all directions with varying amplitudes and phases. The scattering phenomenon that occurs and the particular method used to perform RCS predictions are characterised by the relationship between the wavelength λ and the "characteristic dimensions" of the body. Consider, for instance, the classical

case of a conducting sphere where the circumference $2\pi a$ plays the role of the characteristic dimension. Three distinct regions are characterised by the ratio $2\pi a/\lambda$. At low frequencies, for which the wavelength λ is much greater than the circumference of the sphere, the RCS is proportional to $(2\pi a/\lambda)^4$. At low frequencies, σ is small, but increases with the fourth power of frequency. When the frequency is such that $1 < 2\pi a/\lambda < 10$, the cross-section curve exhibits very distinct oscillatory behaviour. This region of values of circumference to wavelength is known as the *resonance region*. When $2\pi a/\lambda > 10$ (i.e., when the wavelength is much smaller than the circumference), the oscillations decrease, and the curve approaches a constant value of πa^2, which is the projected area of the sphere. Three general frequency intervals like those described above for the sphere, are characteristic of all bodies [5, pp. 39–87]; [6, pp. 11.1–11.56].

(i) *Low-frequency scattering*: When the wavelength of the incident field is much larger than the characteristic dimensions of the body (the so-called *Rayleigh scattering*) there is essentially no phase variation of the incident field over the entire scattering body; the latter is immersed in the same incident field at any given instant of time, in much the same way as in a static field problem. The major feature of Rayleigh scattering is that the cross section is proportional to the fourth power of frequency, as in the case of the sphere for low circumference to wavelength. Furthermore, the scattering is directly dependent on the volume of the scatterer and only weakly dependent on its specific shape [5]. This is the reason why the RCS reduction technologies based on the shaping of the target (see [1, p. 457]) are not effective in the low-frequency region. This frequency region is of interest in this paper because is this where the LFR is supposed to operate.

(ii) *Resonance region scattering*: When the wavelength of the incident field is of the same order as the characteristic dimensions of the body, the phase of the incident field will change appreciably over its length. The range of body size-to-wavelength ratios for which this occurs defines the resonance region. The total field at any point on the body is the sum of the incident field plus an induced field arising from the currents and charges induced by the incident field on all other parts of the body [5, pp. 39–87]; [6, pp. 11.1, 11.56]. This frequency region might be of interest to our work even tough the exact relationship between the target length and the electromagnetic wavelength is not known a priori and cannot be precisely exploited to improve the radar detection.

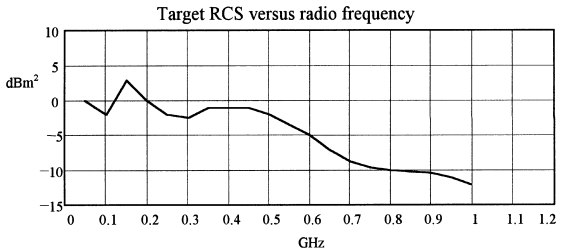

Fig. 2. RCS (in dB m^2) versus frequency for a generic target seen at $\pm 60^\circ$ from nose-on (with permission, from [3]).

(iii) *High-frequency scattering*: When the wavelength of the incident field is much smaller than the characteristic dimensions of the body, collective interactions between scattering centres are insignificant, so that the aggregate body may be treated as a collection of independent, individual scattering centres. The RCS reduction technologies have been concentrated in this frequency region (containing the L, S, C, and X bands) which is where the conventional search and tracking radar operate. Four technologies are in use to reduce the RCS value [5, pp. 39–87]: shaping, radar absorbing material, passive and active cancellation of radar echo. It is claimed that they are effective in this microwave frequency region. We hypothesise that our MR operates at X-band.

A key information for the development of our work is the availability of the target RCS versus frequency, when the latter is spanning from VHF (30–300 MHz, [6, pp. 1.13–1.18]) and UHF (300 MHz–1 GHz) up to microwaves, say X-band (i.e., up to 10 GHz). This information is not readily available in the technical literature especially for target which adopts the above mentioned RCS reduction technologies. Nevertheless, an interesting example, deduced by the literature, is reported in Fig. 2 [3] in the frequency regions of VHF and UHF. In the microwave region, more specifically at

X-band, the target RCS is taken equal to 0.01 m^2; this small numerical value is hypothesised to be obtained by resorting to suitable RCS reduction technologies.

It is readily seen that there are 10–20 dB of difference in RCS between the low frequency (hundreds MHz) and the microwave (GHz range) regions; this RCS advantage motivates the better detection capability of the LFR with respect to the MR. The function $\sigma = f(\lambda)$ will be used in the radar equation to determine the ranging capability of the LFR.

3. Sensor fusion problem

The maximum range at which a target can be detected is given by the classical radar equation [6, p. 1.7]

$$R_{\max}^4 = \frac{P_t A_e^2 \sigma}{4\pi\lambda^2 S_{\min}}, \tag{1}$$

where P_t is the average transmitted power, A_e the effective receiving aperture, σ the target radar cross-section, λ the wavelength of radar electromagnetic wave, and $S_{\min}$ the minimum signal-to-noise power ratio related to prescribed values of detection and false alarm probabilities.

Once the target is detected, it is located in angle (either azimuth or elevation) with an accuracy depending on the SNR and the half-power beam width [6, pp. 9.30, 7.12]

$$\sigma_\theta = C\frac{\theta_B}{\sqrt{\mathrm{SNR}}}, \tag{2}$$

$$\theta_B = \frac{50.8}{d/\lambda} \quad \text{(deg)}, \tag{3}$$

where σ_θ is the standard deviation of angle measurement, C a suitable constant, θ_B the half-power beam width, and d the effective antenna aperture.

Apply (1)–(3) to MR: the σ value is small (0.01 m^2), thus $R_{\max}$ is also small; when the target has been detected, the target is located with a small σ_θ; i.e., the angular location is accurate. Apply (1)–(3) to LFR: the σ value is high (say, 1 m^2, see Fig. 2), consequently $R_{\max}$ is greatly increased; but the target angular location accuracy is poorer than the one achieved by the MR. In fact, assuming A_e be equal for MR and LFR, the corresponding θ_B increases of a factor 100 at 100 MHz with respect to 10 GHz. The target location accuracy in range is related to the transmitted pulse duration and the SNR. In this paper it is assumed that both the two radar have comparable location accuracy in range; thus, the paper will concentrate on the angular location accuracy problem.

The proposed integration of the two radar is depicted in Fig. 3.

The LFR starts scanning the surveillance space with a fan beam wide in azimuth and in elevation; say: the half-power beam width in azimuth is $\theta_B = 40^\circ$, the half-power beam width in elevation is $\phi_B = 85^\circ$. When the target is detected in a certain angular sector Ω (see Fig. 2), this information is passed, via the manager of the integrated system, to the beam scheduler of MR. The microwave phased-array radar starts concentrating its radiated energy within the sector Ω sweeping the narrow beam across it. The target will eventually be detected; a track will also be initialised and updated. These information are displayed on the man–machine interface.

4. Detection range without and with cueing

In this section, we compare the detection capability of the MR and LFR operating in isolation and in the fused mode as sketched in Fig. 3. Start by writing the pertinent equations; subsequently, apply them to a numerical example that will be further developed in the next sections of the paper.

The range at which a target is detected is given by the radar equation (1) when the target is in free space; a refined equation takes into account also the various sources of SNR losses (atmospheric, beam shape, transmitting, receiving, processing, antenna power efficiency). Thus, the radar equation becomes [6, p. 9.29]

$$R = \left[\frac{P_t A_e \sigma t_f U_s}{4\pi K_B T S_{\min} L \Omega_o}\right]^{0.25}, \tag{4}$$

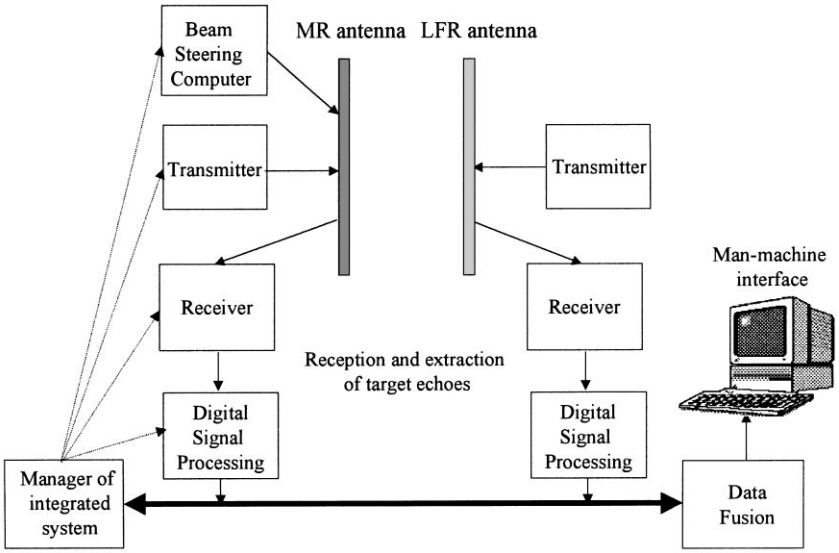

Fig. 3. Integration scheme of MR and LFR.

where R is the range of the radar, t_f is the refresh time period for a given angular sector Ω_o, U_s is the time fraction dedicated to the search function (e.g., 0.4 is dedicated to the search and the remaining to the track initiation and track maintenance), K_B ($1.381\,10^{-20}$ mW/Hz K) is the Boltzmann constant, T (K) is the noise temperature of the radar receiver, L is the global losses (including atmosphere, beam shape, etc.) of radar, and Ω_o is the overall search volume (e.g., 360° in azimuth and, say, 85° in elevation).

Note that $U_s = 0.4$ corresponds to heavy system load. This is a common procedure to design a MR system in a multitarget environment. Note also that passing from $U_s = 0.4$ to 1 corresponds only to 20% of increase of the radar range.

The S_{min} is calculated by the following equation which applies to the case of Swerling 1 target model [5, p. 192]:

$$S_{min} = \frac{\ln P_{FA}}{\ln P_D} - 1, \tag{5}$$

where P_D and P_{FA} are the required detection and false alarm probabilities, respectively; current numerical values are $P_D = 0.8$ and $P_{FA} = 10^{-6}$ corresponding to $S_{min} = 17.8$ dB.

In reality, the acquisition range of the target is limited by the horizon of the Earth and the multipath. The equation that describes the radar range limitation for the presence of the horizon is

$$R_h = \sqrt{2 \times \tfrac{4}{3} R_{EARTH}}(\sqrt{h_R} + \sqrt{h_{tgt}}) = 4120(\sqrt{h_R} + \sqrt{h_{tgt}}) \quad \text{(m)}, \tag{6}$$

where R_h is the maximum radar range in presence of a spherical Earth, R_{EARTH} is the Earth radius, h_R is the height of the radar phase centre, and h_{tgt} is the target height above the Earth surface.

The equation that gives the radar range limitation in presence of target multipath is (see the appendix)

$$R_m = \frac{4\pi h_R h_{tgt}}{0.3/f_c \text{ (GHz)}}, \tag{7}$$

where R_m is the maximum radar range in presence of multipath.

In fact, when the target reflects two paths (the direct and the reflected which interfere) the detection capability of the radar may be severely affected; the equation above gives the maximal radar range in presence of this destructive phenomenon. The dependence on λ says that the multipath

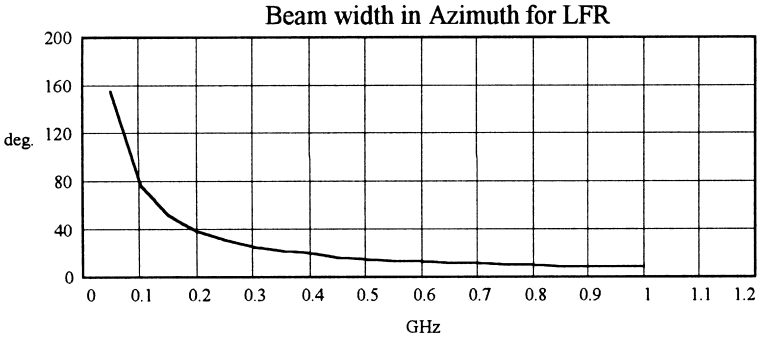

Fig. 4. Half-power beam width in azimuth of the LFR versus carrier frequency.

limitation is more severe for the LFR than for the MR.

The final radar ranging capability will be established by the minimum among the values provided by Eqs. (4), (6) and (7). This calculation procedure is applied both to the MR and to the LFR when they operate alone.

Note that for the LFR the numerical value of U is equal to one because the LFR need not perform any dedicated tracking activity. Another point to clarify is that the carrier frequency of the LFR is a parameter of the study, thus the resulting radar range will be depicted as a function of this carrier frequency.

The carrier frequency of LFR determines the beam width of the radiation pattern. Assume that for practical reasons the horizontal length of the LFR antenna is, say, $d_x = 2$ m, the corresponding half-power beam width in azimuth is

$$\theta_{\mathrm{B,LFR}}\ (\mathrm{deg}) = \frac{50.8}{d_x}\lambda. \tag{8}$$

Fig. 4 depicts the $\theta_{\mathrm{B,LFR}}$ versus LFR frequency.

The vertical width d_y of the LFR antenna is determined in order to cover a specified elevation sector, say 85°. The maximum allowable value of d_y is, for operational reasons, set to 2 m. The area of the LFR antenna aperture becomes function of the LFR frequency as shown in Fig. 5; this function will be exploited in Eq. (4) to determine the ranging capability of the LFR.

A word of comment on the figure seems proper. Low-frequency search radar antenna dimensions are not fixed. Aperture width is constant and equal to 2 m. Aperture height varies according the following criteria:

- it is limited to a maximum value that corresponds to the specified elevation coverage (85°) for each transmission frequency;
- it must be further reduced if it exceeds 2 m (however coverage specification is still satisfied).

Therefore, the overall aperture area grows towards lower frequency (as shown in Fig. 5), but it is limited to a maximum 4 m^2 (see working hypotheses), following the law

$$A_{\mathrm{eff}}(f) = 2\min\left(0.9\frac{\lambda}{\theta_{\mathrm{El}}},2\right)\quad(\mathrm{m}^2). \tag{9}$$

The real detection range of the LFR must also take into account the random delay between the time when the target enters the coverage volume and the time when the beam is aimed at; an average delay value corresponding to half-radar antenna rotation period is considered.

The ranging capability of the MR cued by the LFR is calculated as follows. The acquisition range is computed in the conservative hypothesis of scanning the whole cueing sector Ω in order to acquire the target. The target is supposed to approach the radar site along a radial trajectory with constant velocity; as a consequence the acquisition range of the MR cued by the LFR is the acquisition range of the LFR minus the distance travelled by the target during the time needed by the MR beam to scan the whole sector Ω where the LFR has detected the target.

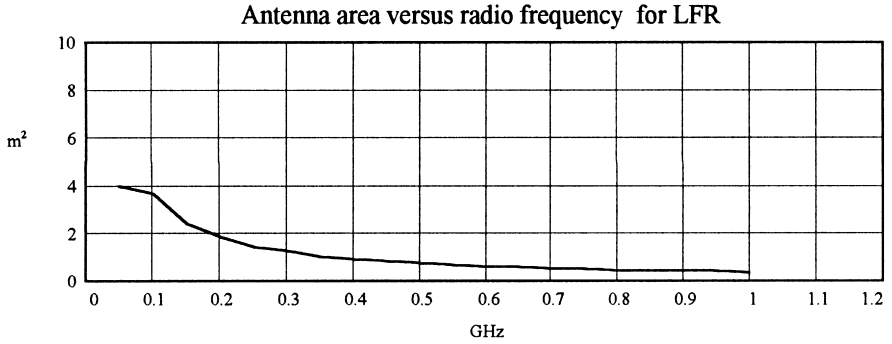

Fig. 5. Area of the LFR antenna aperture versus carrier frequency.

In the following we present the results of the application of Eqs. (4), (6) and (7) to three systems:
(i) MR in stand-alone mode,
(ii) LFR in stand-alone mode, and
(iii) MR cued by the LFR,
for a numerical study case that will be further developed in the next sections of the paper.

4.1. Working hypotheses

- The MR and LFR are placed in the same site.
- The MR is a multifunction phased-array operating at 10 GHz. Its antenna rotates mechanically in azimuth; the beam can be pointed electronically in both azimuth and elevation. Azimuth pointing is possible within $\pm 45^\circ$ off the current boresight azimuth. When operating in a stand alone mode, the radar dedicates a prescribed time fraction (U_s in Eq. (4)) to search.
- MR performs cued acquisition in the angle sector corresponding to the LFR azimuth beamwidth.
- The LFR has a mechanical rotating fan beam antenna that dedicates the whole time to search ($U_s = 1$ in Eq. (4)). The operating frequency is in the VHF–UHF regions; the precise value will be a result of the following analysis. LFR does not provide elevation.
- Both MR and LFR ensure the same angular coverage in azimuth and elevation.
- For operational reasons, the dimension of the LFR and MR antennas should not exceed prescribed limits, say 2 m × 2 m.

4.2. Parameters of the target

The target RCS is the one depicted in Fig. 2 in the low-frequency region; it is equal to 0.01 m^2 at X-band. The target trajectory is radial towards the radar site; the target altitude of flight is $h_{tgt} = 3000$ m; the approaching velocity is 300 m/s.

4.3. Parameters of the MR

The height of the antenna phase centre above the Earth surface is $h_{MR} = 3.5$ m. The average transmitted power is $P_{t,MR} = 77$ dB mW. The antenna aperture is 2 m × 2 m. The carrier frequency is 10 GHz. The half-power beam width in azimuth and in elevation are 0.8° and 1.2°, respectively. The antenna scan period is 1 s. The refresh time t_f for the overall search volume (360° in azimuth and 85° in elevation) is 5 s. The time fraction U_s dedicated to search is 0.4; the time fraction dedicated to track initiation and track maintenance is 0.6. The receiver noise temperature is $T_{MR} = 1000$ K. The whole losses amount to $L_{MR} = 11$ dB. The prescribed detection and false alarm probabilities are 0.8 and 10^{-6}, respectively. The allowed dwell time for track initiation is 3.2 ms, while the dwell for track maintenance is 12.8 ms.

4.4. Parameter of the LFR

The height of the antenna phase centre above the earth surface is $h_{LFR} = 3.5$ m. The average transmitted power is $P_{t,LFR} = 80$ dB mW. The antenna

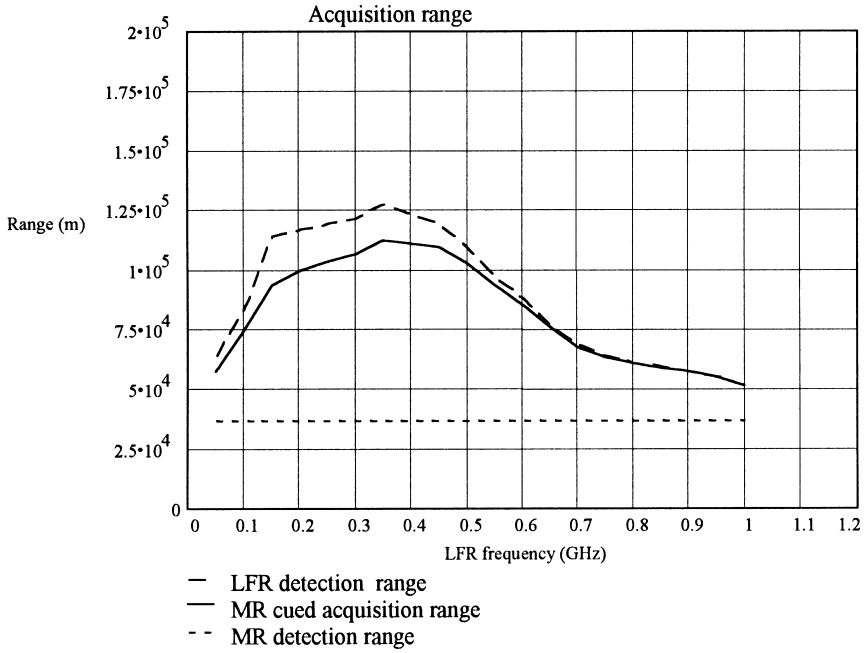

Fig. 6. Comparison of the target detection range for the LFR alone, the MR cued by the LFR and the MR alone. The detection range is depicted versus the carrier frequency of the LFR.

aperture is at maximum 2 m × 2 m. The antenna scan period is 4 s. The whole scan sector is 360° in azimuth and 85° in elevation. The time fraction U_s dedicated to search is 1. The receiver noise temperature is $T_{LFR} = 1000$ K. The whole losses amount to $L_{MR} = 9$ dB. The prescribed detection and false alarm probabilities are 0.8 and 10^{-6}, respectively.

The numerical values of the parameters of the MR and of the LFR do not refer to any specific system but, rather, are chosen for sake of explanatory example.

4.5. Results

Fig. 6 compares the acquisition range for the LFR in stand-alone mode, the MR cued by the LFR and the MR in stand-alone mode; the acquisition range is drawn versus the carrier frequency of the LFR.

We observe that the detection range of the MR is a constant value, while the detection range of the LFR and of the MR cued by the LFR are functions of the carrier frequency of the LFR. It is also noted that the range of the integrated system is less than the range of the LFR in stand-alone mode. This is due to the fact that the MR antenna has to rotate many times to complete the whole cueing sector Ω. In fact, MR cued acquisition range is computed as follows:

- between LFR detection and MR acquisition start there is an average time delay of half-scan period of MR,
- MR has to acquire the target in the cueing volume Ω provided by LFR,
- the worst case is assumed, that MR has to scan sequentially all the cueing volume to find the target,
- due to antenna rotation of MR and the contemporaneous fulfilment of other concurrent tasks, it is assumed that only, say, 25% of time is available for the acquisition task in a rotation period,
- the target radar cross-section has a much lower value at MR frequency, than at LFR;

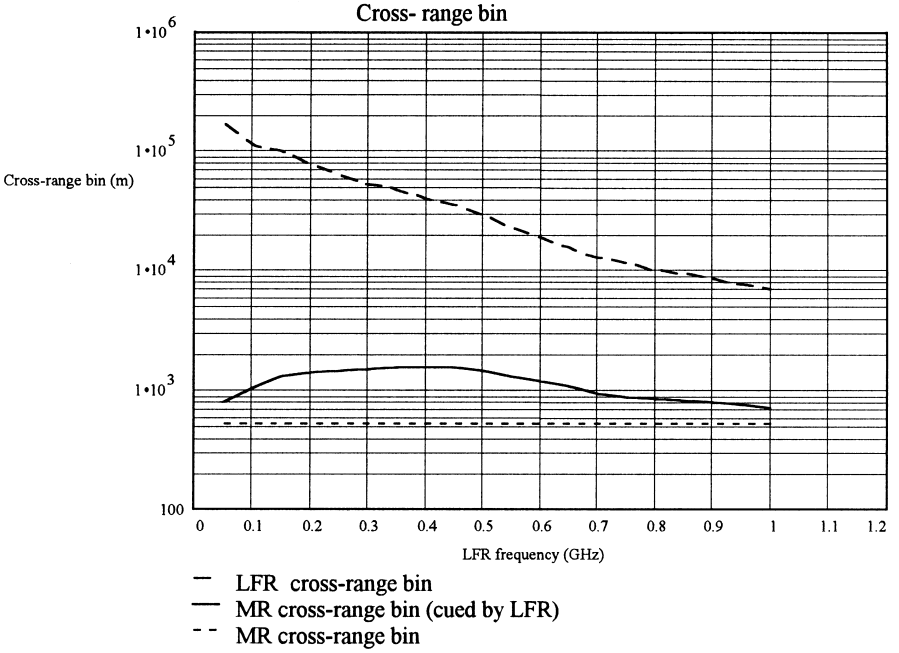

Fig. 7. Comparison of the cross-range location accuracy for the LFR alone, the MR alone and the MR cued by the LFR. The cross-range location accuracy is depicted versus the carrier frequency of the LFR.

consequently, MR must dwell more time along the target direction to reach the same $P_D = 0.8$ of LFR.

A question might arise concerning the capability of the cued MR to localise and detect the target although it is still out of the MR detection range in the stand-alone mode. The answer is that the acquisition time is made long enough to allow detection of MR with prescribed P_D and P_{FA} values. This is possible because MR is made free from search task and it can devote all available time to acquisition and tracking tasks.

There is a maximum of the range at the frequency equal to 0.35 GHz that does not exactly coincide with the frequency where the target RCS has the peak; however, the maximum is quite flat in the frequency interval 0.15–0.5 GHz which corresponds to the same interval where the target RCS is high.

The cross-range accuracy (in the azimuth direction) for systems (i)–(iii) in locating the target is given by the following equations:

$$\sigma_{cr,MR} = \theta_{B,MR} R_{MR},$$
$$\sigma_{cr,MR\ cued}(f) = \theta_{B,MR} R_{MR\ cued}(f), \quad (10)$$
$$\sigma_{cr,LFR}(f) = \theta_{B,LFR} R_{LFR}(f),$$

where R_{MR}, $R_{MR\ cued}$ and R_{LFR} are given in Fig. 6. Fig. 7 compares the cross-range accuracy for the three radar systems.

It is noted that the location accuracy of the integrated system is far more better than the accuracy of the LFR in stand-alone mode; the accuracy is approximately constant in the frequency interval 0.15–0.55 GHz. Thus, it is shown that the integrated system combines the good detection of the LFR and the good location capability of the MR.

5. Track initiation without and with cueing

Once the target is detected, the track initiation is started at the subsequent scan period for the MR

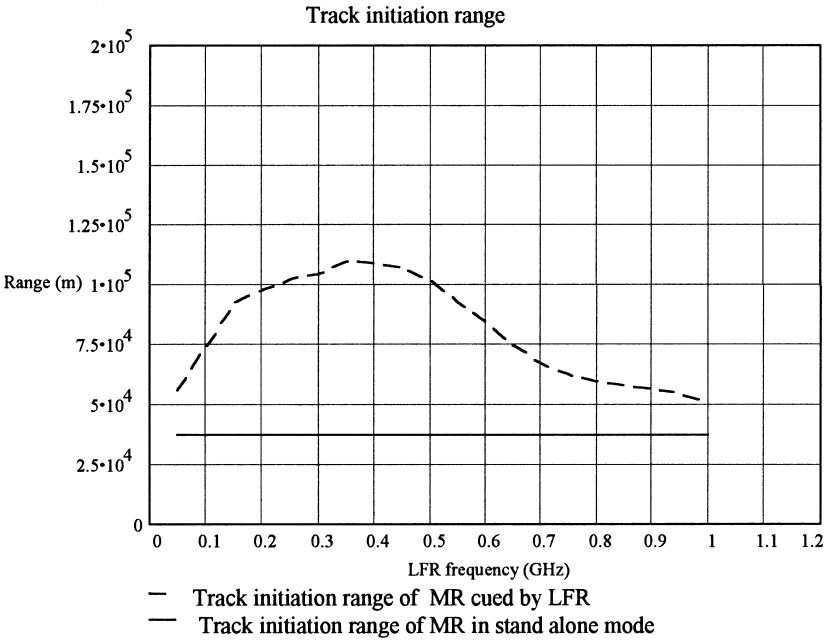

Fig. 8. Track initiation range for the MR alone and the MR cued by the LFR. The track initiation range is depicted versus the carrier frequency of the LFR.

operating in stand-alone mode and in cued mode. The theory of track initiation is extensively described in [2, pp. 203–210]. The current procedure to initialise a track is based on the so-called "M out of N" logic; i.e., if M detections occur out of N consecutive scans, with $N \geqslant M$, the track is successfully initialised. The calculation of the probability of successfully initiate a track is done by resorting to the Markov chain theory. Consider the logic "2 out of 3"; a Markov model of this logic envisages several states having the content "$i\ j\ k$" where $i,j,k = 0,1$ represent the detection occurrence or the absence of detection at a certain scan. Example: "1 0 0" means detection occurrence at the first scan and no detection at the second and third scans. The evolution of the Markov chain is governed by the detection probability which in turn depends on the SNR value along the target path. The probability of track initiation is calculated by the probability to reach the Markov state having two ones out of three. We require 0.95 of probability to have a successful initiation of the track. The track initiation range is obtained by the range at which the probability of track initiation is 0.95. The track initiation range is calculated for the MR alone and for the MR cued by the LFR; Fig. 8 depicts the ranges versus the carrier frequency of the LFR. The two curves differ by the different values of the acquisition range (see Fig. 6). Fig. 8 pertains to the same numerical example developed in Section 4.

The cross-range accuracy at the track initiation range can be calculated by applying Eq. (10) provided that the range is the track acquisition range. Fig. 9 displays the cross-range accuracy for the MR and the MR cued by the LFR versus the carrier frequency of the LFR.

Fig. 8 shows the benefit of adopting the integrated radar system; there is a maximum of tracking initiation range at 0.35 GHz. Fig. 9 indicates the degradation of the cross-range accuracy of the integrated system with respect to the MR operating in stand-alone mode.

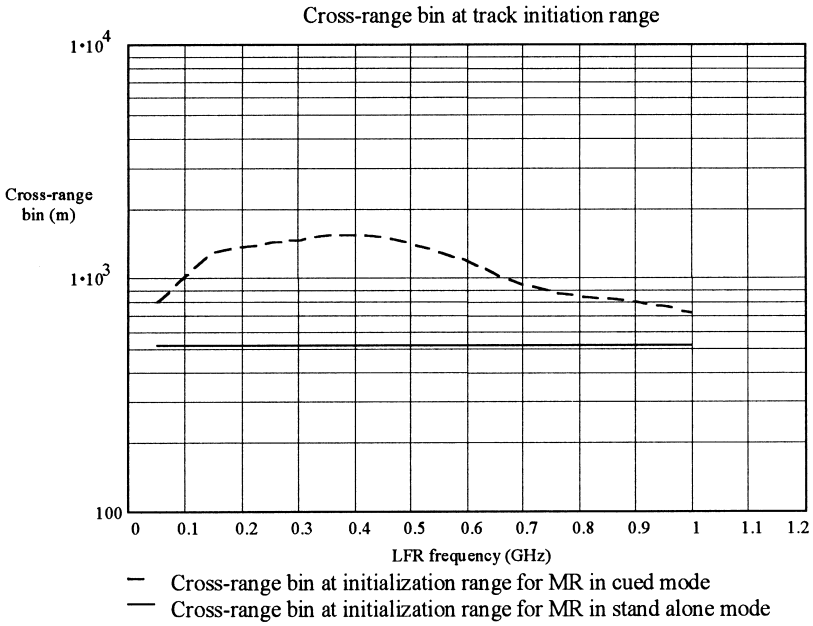

Fig. 9. Cross-range accuracy at the track initiation range for the MR in stand-alone mode and the MR cued by the LFR. The cross-range accuracy is depicted versus the carrier frequency of the LFR.

6. Track accuracy without and with cueing

Once the track is initiated, it is maintained by periodically steering the radar beam along the predicted radar–target line of sight and processing the corresponding radar measurements by means of a suitable tracking filter.

Initial target position estimate might be affected by large errors because the MR is working outside its maximum range in stand alone mode. Nevertheless, the target is correctly located because more radar time is dedicated to the measurement of the target spatial co-ordinates. This is possible because the search function has been executed by the LFR in lieu of the MR. To locate the target, a solid angle containing more than one MR resolution cell is scanned. This is done with a cluster of MR beams, placed around the predicted radar–target line of sight, which is scheduled for each tracking update. The uncertainty area will progressively reduce as the number of tracking filter updates increases.

In the present work the tracking filter is built around the Kalman algorithm; the theory and the design of the Kalman algorithm for tracking are extensively described in [2, pp. 165–173]. Here we determine the number of radar scans needed to have a smoothed track with a prescribed value of the cross-range accuracy in azimuth. Thus, we recursively apply the Kalman algorithm to the set of radar measurements and determine the smoothed position and velocity of the target track. We also determine the error standard deviation of the estimated position of the target via the so-called Riccati matrix equation which is one of the key equations in the Kalman algorithm. Fig. 10 gives the target range at which the cross-range accuracy in azimuth is equal to a specified value, 30 m in the numerical example. Fig. 10 has been obtained for the same numerical exercise developed in Sections 4 and 5. The figure gives the tracking range for the MR in stand-alone mode and for the MR in cued mode. It is seen that there is a remarkable advantage using the cueing mode with respect to the stand-alone mode.

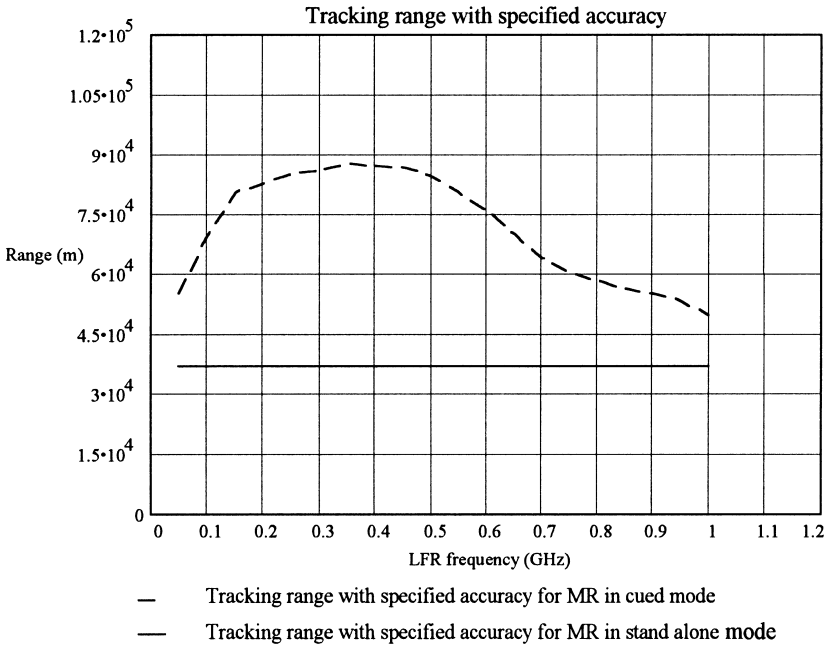

Fig. 10. Range at which the cross-range accuracy has reached the value of 30 m. MR in stand-alone mode and MR in cueing mode. The tracking range is shown versus the carrier frequency of the LFR.

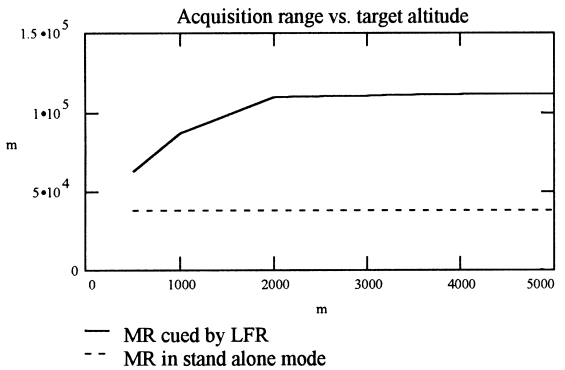

Fig. 11. Acquisition range versus the target height of flight for the two compared systems: the MR cued by the LFR and the MR in stand alone mode.

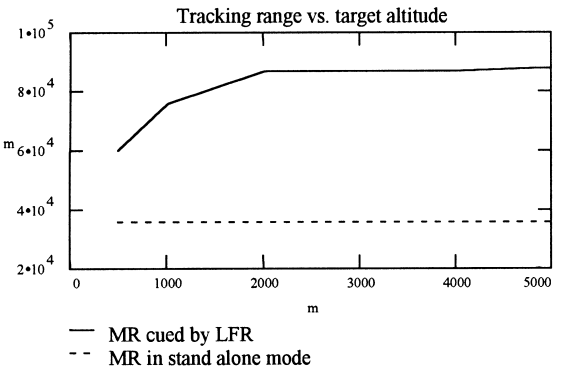

Fig. 12. Tracking range versus the target height of flight for the two compared systems: the MR cued by the LFR and the MR in stand alone mode.

7. The problem of multipath

As already pointed out the LFR is affected by multipath. To evaluate the entity of this phenomenon we report in Figs. 11 and 12 the acquisition and the tracking range versus the target height of flight for the two systems: MR in stand alone mode and MR in cued mode. The figures are based on the multipath model described in the appendix. We note that the multipath effect is less detrimental as

the target height of flight increases; the multipath does not affect the performance of the MR in stand alone mode.

8. Concluding remarks

In this paper we have studied an integrated system made of two radar, one operating at microwave and the other operating at low frequency. The rationale is to combine the advantages of having a large target RCS value in the low frequency with the good location accuracy of the microwave radar. The working mode of the integrated system was illustrated; the performance of the system was compared to the performance of MR in stand-alone mode.

The main benefit of LFR cueing consists in anticipated detection of dim targets, because of comparatively larger radar cross-section, and reduction of radar time that is devoted to search. On the other hand, MR must spend more time during acquisition, track initiation and initial tracking phase of a target with small radar cross section (at microwave frequency). Overall, there is a time saving when the MR is cued by LFR. In fact, both radar are optimised for their specific tasks; more precisely, LFR is optimised for search task (because it radiates a frequency where the target RCS is higher), while MR is optimised for acquisition and tracking tasks (because the higher transmitting frequency is more suitable to reach the final localisation accuracy).

A detailed numerical example was carried out. For that example it was shown that the carrier frequency of the LFR should be in the region 0.15–0.5 GHz (see Fig. 10). On the basis of the analysis done and the selected RCS (f) function for the numerical example developed above, it has been found that the best value for the carrier frequency of the LFR is 350 MHz. In fact, the integrated system achieves a detection range of 112 km ($P_{\mathrm{D}} = 0.8$ and $P_{\mathrm{FA}} = 10^{-6}$), a track initiation range at 110 km, a tracking range at 88 km (at which the cross-range tracking accuracy is 30 m) in lieu of a detection range, a track initiation range and a tracking range (with cross-range tracking accuracy equal to 30 m) all approximately equal to 37 km for the MR in absence of cueing.

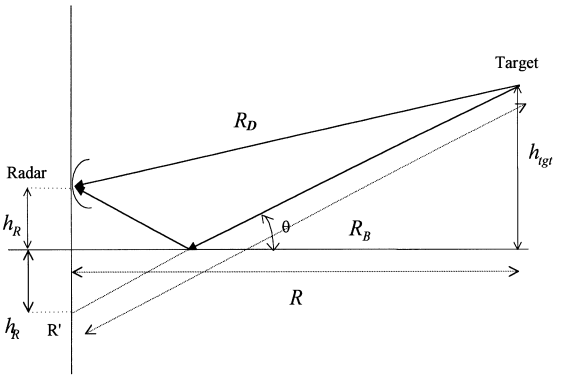

Fig. 13. Multipath model.

A limitation of the integrated system is represented by the multipath that affects the ranging capability of the LFR. An infrared search and tracking system (to integrate with the two radar) could provide the horizon coverage due to the infrared immunity to multipath; but the background noise (natural and man-made either intentional or not) might degrade significantly the system performance. An alternative is a radar operating at a frequency lower than the VHF to exploit the propagation guided by the terrain to detect low elevation target [7]. The fusion of data by these three radar operating at such different carrier frequencies is a matter for future studies.

Acknowledgements

The authors acknowledge the careful revision of the paper by two referees; their suggestions have improved the paper.

Appendix

A simple flat earth multipath model with perfect reflection is used as shown in Fig. 13.

The radar is at a height h_{R} above the reflecting surface and an image radar (R') is placed at an equal distance below the reflecting surface. The

signal $\boldsymbol{E}$ received by the radar is the combination of the $\boldsymbol{E}_{\text{direct}}$ and the $\boldsymbol{E}_{\text{bounce}}$; the phase of the image radar is negated due to the phase flip on reflection [4]. Target echo is reduced (or amplified) by the following coefficient:

$$F_{\text{P}}^4 = \frac{|\boldsymbol{E}|^4}{|\boldsymbol{E}_{\text{direct}}|^4} = \frac{|\boldsymbol{E}_{\text{direct}} - \boldsymbol{E}_{\text{bounce}}|^4}{|\boldsymbol{E}_{\text{direct}}|^4}$$

$$= \frac{|\mathrm{e}^{-\mathrm{j}2\pi R_{\text{D}}/\lambda} - \mathrm{e}^{-\mathrm{j}2\pi R_{\text{B}}/\lambda}|^4}{|\mathrm{e}^{-\mathrm{j}2\pi R_{\text{D}}/\lambda}|^4}$$

$$= |1 - \mathrm{e}^{-\mathrm{j}2\pi\Delta R/\lambda}|^4 = 16\sin^4\left(\pi\frac{\Delta R}{\lambda}\right). \tag{A.1}$$

The path difference ΔR is given by

$$\Delta R = R_{\text{B}} - R_{\text{D}}$$

$$= \sqrt{R^2 + (h_{\text{tgt}} + h_{\text{R}})^2} - \sqrt{R^2 + (h_{\text{tgt}} - h_{\text{R}})^2}$$

$$= \frac{4h_{\text{R}}h_{\text{TGT}}}{\sqrt{R^2 + (h_{\text{tgt}} + h_{\text{R}})^2} + \sqrt{R^2 + (h_{\text{tgt}} - h_{\text{R}})^2}}$$

$$\cong \frac{2h_{\text{R}}h_{\text{TGT}}}{R} \tag{A.2}$$

The propagation factor F_{P}^4 is zero when

$$\Delta R = k\lambda \tag{A.3}$$

with k any integer value. The propagation factor F_{P}^4 is one when

$$\Delta R = \frac{\lambda}{6} \tag{A.4}$$

or

$$R = \frac{12h_{\text{R}}h_{\text{tgt}}}{\lambda}. \tag{A.5}$$

For long ranges, the propagation factor F_{P}^4 can be approximated as

$$F_{\text{P}}^4 \approx \left(\frac{4\pi h_{\text{R}}h_{\text{tgt}}}{R\lambda}\right)^4 = \left(\frac{R_{\text{m}}}{R}\right)^4, \tag{A.6}$$

where

$$R_{\text{m}} = \frac{4\pi h_{\text{R}}h_{\text{tgt}}}{\lambda} = \frac{4\pi h_{\text{R}}h_{\text{tgt}}}{0.3/f_{\text{c}}\ (\text{GHz})} \tag{A.7}$$

which corresponds to (7). From (A.6) we conclude that when the target range R is greater than R_{m}, the multipath limitation is very strong; thus, in practice, R_{m} is the maximum target range in presence of multipath.

The above simplified model has been introduced to show range limitations caused by multipath without taking into consideration the oscillatory nature of the pattern in the interference zone. Thus, the resulting multipath model has been simplified as follows:

- Eq. (A.6) is applied when $R > R_{\text{m}}$;
- the propagation factor F_{p}^4 is approximated – on the average – to one when $R \leqslant R_{\text{m}}$.

References

[1] E. Brookner, Aspects of Modern Radar, Artech House, Boston, MA, 1988.

[2] A. Farina, F.A. Studer, Radar Data Processing. Introduction and Tracking, Vol. I, Researches Studies Press, England, 1985.

[3] H. Kuschel, VHF/UHF radars: einsatzbereich und beschrankungen, 1997, CCG, Carl Krantz Gesellschaft e.v. (Fig. 19).

[4] M.W. Long, Radar Reflectivity of Land and Sea, Artech House, Boston, MA, 1983.

[5] W. Morchin, Airborne Early Warning Radar, Artech House, Boston, MA, 1990.

[6] M.I. Skolnik, Radar Handbook, 2nd Edition, McGraw-Hill, New York, 1990.

[7] www.sunspot.nosc.mil.